Extrinsic optical-fiber ultrasound sensor using a thin polymer film as a low-finesse Fabry–Perot interferometer

P. C. Beard and T. N. Mills

Theoretical and experimental aspects of an extrinsic optical-fiber ultrasound sensor are described. The sensor is based on a thin transparent polymer film acting as a low-finesse Fabry–Perot cavity that is mounted at the end of a multimode optical fiber. Performance was found to be comparable with that of a piezoelectric polyvinylidene difluoride-membrane (PVDF) hydrophone with a sensitivity of 61 mV/MPa, an acoustic noise floor of 2.3 KPa over a 25-MHz bandwidth, and a frequency response to 25 MHz. The wideband-sensitive response and design flexibility of the concept suggests that it may find application as an alternative to piezoelectric devices for the detection and measurement of ultrasound.

Key words: Optical fiber, ultrasound, Fabry–Perot, polymer film.

1. Introduction

The detection of ultrasound is most commonly achieved by the use of piezoelectric devices. Transducers made from piezoceramics such as lead zirconate titanate (PZT) and lithium niobate ($LiNbO_3$) can offer high sensitivity, but their poor acoustic-impedance match to liquids results in a very nonuniform frequency response, giving a poor representation of the detected signal. The piezoelectric polymer polyvinylidene difluoride (PVDF) has an acoustic impedance much closer to that of water, thus giving a more uniform frequency response, but it is not as sensitive as piezoceramic devices. Common to transducers fabricated from both types of material are a susceptibility to electromagnetic interference and signal distortion and a reduced sensitivity that is due to the electrical-loading effects of the transducer leads. In addition, the cost and fragility of piezoelectric-transducer elements limit their use for certain applications.

Various intrinsic and extrinsic optical-fiber ultrasound sensors have been suggested as an alternative to piezoelectric devices for applications in which a totally electrically passive sensor is required. Intrinsic ultrasound sensors, in which the fiber itself acts as the transduction element, have tended to be either polarimetric[1–6] or interferometric[7–10] devices. Although intrinsic sensors have been demonstrated to be capable of detecting acoustic waves at ultrasonic frequencies, their sensitivity is relatively low compared with that of piezoelectric transducers. Their uniformity of frequency response is also poor because of the acoustic-impedance mismatch between the fused silica of the optical fiber and water.[7] A further limitation for applications in which a high degree of measurement accuracy is required arises from the fact that the active length of the fiber responds to the line integral of the acoustic field.[3] If the phase of the ultrasound field over the region intercepted by the fiber is not the same at all points along the fiber, the peak pressure of the field may be underestimated. In addition, active phase-control[11] and polarization-control[12] systems are often required to keep the sensor at its optimum operating point, adding to the cost and complexity of the system. For point measurements for which a probe-type configuration is required, intrinsic optical-fiber sensors are generally unsuitable because a length of fiber, typically close to 1 cm, must be placed in the ultrasound field. Extrinsic optical-fiber ultrasound sensors are more suitable in this respect. These sensors use the fiber simply to deliver light to and from an optical sensor at the end of the fiber, which interacts with the acoustic field. One scheme relies upon the interferometric detection of acoustically induced changes in the separation of two optical fibers in a silica tube.[13] Another that uses a fiber

The authors are with the Department of Medical Physics and Bioengineering, University College London, Shropshire House, 11-20 Capper Street, London WC1E 6JA, United Kingdom.

Received 1 August 1995.
0003-6935/96/040663-13$06.00/0

Micheleson interferometer[14] is essentially a fiber-optic version of a bulk optical scheme used for the primary calibration of ultrasonic hydrophones.[15] This scheme is based on the measurement of acoustically induced displacements of a thin membrane. High sensitivity has been reported, although a somewhat complex, active phase-bias-control system is required as both arms of the fiber interferometer are sensitive to ambient thermal and pressure fluctuations. Other extrinsic optical-fiber sensors have made use of beam-deflection techniques,[16] Raman–Nath diffraction,[17] and acoustically induced changes in the refractive index at a poly(methyl methacrylate)–water [(PMMA)–water] interface.[18] Most of these extrinsic noninterferometric optical-fiber techniques are of low sensitivity.

The extrinsic optical-fiber sensor described in this paper is based on the detection of acoustically induced changes in the thickness of a thin, clear, polymer film acting as a low-finesse Fabry–Perot interferometer[19] that is mounted at the end of an optical fiber. The use of a thin polymer film as the sensing element has a number of advantages. Because the polymer film itself is the interferometer and has a short path length, it exhibits a low sensitivity to environmental thermal and pressure fluctuations. Thus there is no need for complex polarization- and phase-bias-control systems. A film thickness of a few tens of micrometers gives a megahertz bandwidth and removes the need for a long-coherence source. The low Young's modulus (4–5 GPa) of many polymers as compared with that of a fused-silica (~70–GPa) fiber produce a high acoustic sensitivity. In addition, many polymers have an acoustic impedance close to that of water, resulting in a uniform frequency response. Furthermore, because the active area of the sensor is defined by the core diameter of the optical fiber, small active areas are possible. A small active area avoids the line-integral-response problem of intrinsic sensors and enables a high spatial resolution and a low directional sensitivity to be achieved. In this paper the theoretical aspects of the sensor's performance are considered. This is followed by a comparison of the experimentally measured performance with that of a PVDF-membrane hydrophone.

2. Principles of Operation

A schematic drawing of the system for the optical-fiber detection of ultrasound in water is depicted in Fig. 1. Light from a wavelength-tunable laser diode is launched into a multimode optical-fiber downlead. The sensing element, mounted at the end of the fiber, comprises a thin (typically a few tens of micrometers thick) transparent polymer film acting as a low-finesse Fabry–Perot interferometer. The optical reflection coefficients of the mirrors of the interferometer are defined by the Fresnel reflection coefficients arising from the refractive-index mismatches between the two sides of the film and the surrounding media. This concept avoids the need for optically reflective coatings to be applied to the film. The stress that is due to an incident acoustic wave modulates the thickness of the film, and therefore the optical phase difference between the two reflections. A corresponding intensity modulation is produced, which is then transmitted back along the fiber for detection at a photodiode. For optimum sensitivity and linearity the sensor is operated and maintained at quadrature by adjustment of the wavelength of the laser diode. The space between the fiber tip and the sensing film is filled with water. With the assumption that the sensor is used to detect ultrasound in water, this water-filled cavity serves two purposes. First, the Fresnel reflection coefficients on either side of the film will be equal, giving an optimum fringe visibility of unity. Second, the water provides an acoustic-impedance match on the fiber side of the film, minimizing acoustic reflections that would otherwise degrade the sensor's uniformity of frequency response.

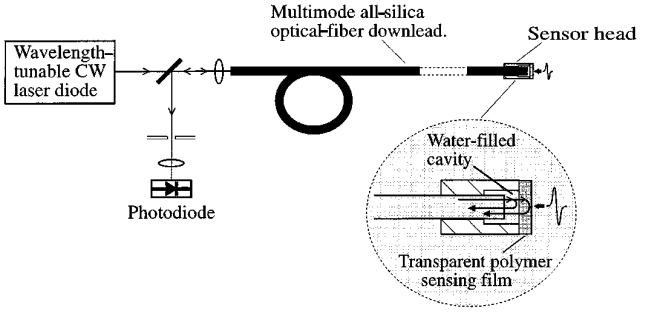

Fig. 1. Schematic diagram showing the optical-fiber detection of ultrasound.

3. Theory

The theoretical aspects of the sensor's operation are considered first with an examination of the output of a low-finesse Fabry–Perot interferometer to obtain the phase sensitivity. Second, the acoustic sensitivity and the frequency response of the sensor are modeled by means of a consideration of the interaction of the sensing film with an acoustic field. Finally the interferometric and acoustic parameters are brought together to give the overall system sensitivity.

A. Low-Finesse Fabry–Perot Interferometer Output

Figure 2 shows a polymer-film sensing element of refractive index n and thickness l in contact with two different media: on the left-hand side medium 1 of refractive index n_1 and on the right-hand side medium 2 of refractive index n_2. The Fresnel reflections coefficients arising from the refractive-index mismatches at the boundaries of the sensing film are assumed to be sufficiently low to permit the contribution of multiple reflections within the interferometer to be neglected. The analysis is therefore that of a two-beam interferometer. In the following subsec-

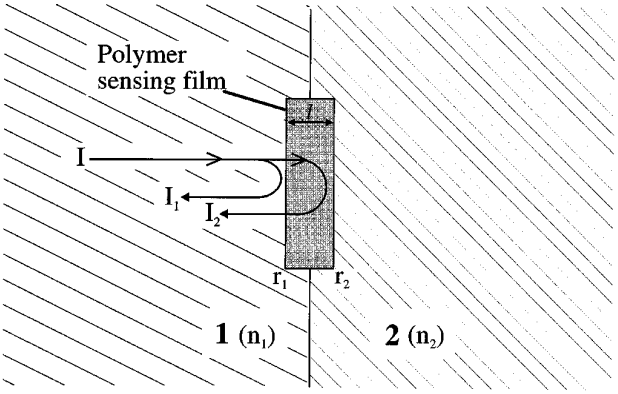

Fig. 2. Diagram of a polymer-sensing film acting as a low-finesse Fabry–Perot interferometer. 1 and 2 denote the media on the left- and right-hand sides, respectively.

tions, the case in which the interferometer is illuminated with light at normal incidence is examined, followed by a consideration of the effects of the illumination of the interferometer with the divergent output of an optical fiber.

1. Illumination of the Sensing Film at Normal Incidence

The resultant intensity I_0 that is due to the superposition of reflections I_1 and I_2 from the two sides of the film as a result of light at normal incidence (Fig. 2) is

$$I_0 = I_1 + I_2 + 2\sqrt{I_1 I_2}\cos\Phi, \tag{1}$$

where Φ is the total phase difference arising from the optical path-length difference between the two reflections. When an acoustic wave is incident on the sensing film, Φ consists of two components: the unsignaled phase-bias term ϕ that defines the working point of the interferometer and a time-varying signal term $d\phi$ that arises from the acoustically induced change in thickness of the sensing film:

$$\Phi = \phi + d\phi. \tag{2}$$

Inserting Eq. (2) into Eq. (1) and expanding give

$$I_0 = I_1 + I_2 + 2\sqrt{I_1 I_2}\cos\phi\cos d\phi - \sin\phi\sin d\phi). \tag{3}$$

For optimum sensitivity and linearity it is desirable that we set the phase-bias term ϕ at quadrature where $\phi = (2m + 1)\pi/2$ (for integer m) by tuning the wavelength of the laser source. At the first quadrature point, $\phi = \pi/2$, and for small $d\phi$, Eq. (3) reduces to

$$I_0 = I_1 + I_2 - 2\sqrt{I_1 I_2}d\phi. \tag{4}$$

Under these conditions, the output of the interferometer that is detected by the photodiode consists of an acoustically induced, time-varying, intensity-modulated term dI_0 that is linearly dependant on $d\phi$ and a dc component I_{dc} by

$$dI_0 = -2\sqrt{I_1 I_2}d\phi, \tag{5}$$

$$I_{dc} = I_1 + I_2. \tag{6}$$

I_1 and I_2 can be written in terms of the incident intensity I and the Fresnel reflection coefficients r_1 and r_2, defined by the refractive-index mismatches at the boundaries of the sensing film by

$$I_1 = Ir_1, \qquad I_2 = I(1 - r_1)^2 r_2, \tag{7}$$

where

$$r_1 = \left(\frac{n - n_1}{n + n_1}\right)^2, \qquad r_2 = \left(\frac{n - n_2}{n + n_2}\right)^2. \tag{8}$$

From Eqs. (5)–(7) the phase sensitivity of the interferometer, defined as the intensity modulation per unit phase shift, $dI_0/d\phi$, and the dc level I_{dc} can now be written as

$$\frac{dI_0}{d\phi} = -2I(1 - r_1)\sqrt{r_1 r_2}, \tag{9}$$

$$I_{dc} = I[r_1 + (1 - r_1)^2 r_2]. \tag{10}$$

It is desirable to maximize the phase sensitivity by a suitable choice of I, r_1, and r_2, but it is important to note that these parameters also affect the dc component. This dc component is an undesirable element of the interferometer output, as it produces a large photocurrent with attendant shot noise that can dominate the noise characteristics of the photodiode. Furthermore, if the dc level is too high it will saturate the photodiode limiting the maximum phase sensitivity that can be achieved by an increase in I. For these reasons it is necessary to both minimize the dc level and maximize the phase sensitivity for optimum performance. This is achieved when values of r_1 and r_2 are chosen that give a fringe visibility of one. For low values of r_1 and r_2 (<1%), such as those defined by the Fresnel reflection coefficients occurring at a polymer–water interface, this condition is met by setting $r_1 = r_2$. This condition can be readily achieved in practice if one ensures that water is in contact with both sides of the film. With the fringe visibility equal to one, the laser power can now be increased as much as possible before it reaches the saturation threshold of the photodiode. This increase enables the highest possible phase sensitivity to be obtained. When a polyethylene terephthalate (PET) sensing film ($n = 1.6$) surrounded by water ($n_1 = n_2 = 1.33$) is used, $r_1 = r_2 = 0.00849$, and for $I =$ 3 mW Eq. (9) yields $dI_0/d\phi = 50.4\ \mu W/rad$. With the use of a typical silicon photodiode, this value of the phase sensitivity would enable phase shifts of the order of 10 mrad to be detected. Equation (10) gives

a value of I_{dc} of 50.4 μW, which is well below the saturation threshold of such a photodiode.

2. *Optical-Fiber Illumination of the Sensing Film*

In a previous paper[19] it was noted that sensitivity decreased significantly when the sensing film was illuminated with the divergent output of an optical fiber. This decrease arises as a result of the increased optical path lengths taken by light at nonnormal angles of incidence.

Consider the case in which a collimated beam of light is normally incident upon the sensing film. All the light that is transmitted into and reflected back from the film travels the same optical path. Each point across the reflected optical field that is due to the interference between the reflections from the two sides of the sensing film is therefore associated with the same phase bias. Thus all the reflected-signal intensity-modulated light dI_0 arriving at the photodiode is in phase. This is in contrast to the situation in which the sensor is illuminated with the divergent light emerging from the end of a large-diameter multimode optical fiber. The optical path length, and therefore the phase bias associated with the reflected light, is dependent on the angle of incidence, and this dependence can lead to conditions in which partial or complete cancellation of the signal occurs. Consider the case in which the light striking the film at normal incidence travels an optical path length $2l$ and assume that this path length corresponds to the first quadrature point. A ray at an angle of incidence θ takes an extra path length Δl:

$$\Delta l = 2l\left(\frac{1}{\cos\theta} - 1\right). \tag{11}$$

The corresponding difference in the phase bias ϕ_d as a result of this extra path length is

$$\phi_d = \frac{4\pi n l}{\lambda}\left(\frac{1}{\cos\theta} - 1\right), \tag{12}$$

where λ is the wavelength of the laser source. As the angle of incidence is increased, the phase-bias difference ϕ_d also increases until $\phi_d = \pi$. At this point the total optical path length corresponds to the next quadrature point and so the intensity-modulated signal is now in antiphase with the signal arising from the normally incident light. When imaged onto the same detector the two signals cancel. This signal-canceling effect not only reduces the phase sensitivity but also adds to the dc level. The solution is to ensure that the thickness of the interferometer and the maximum angle of divergence are such that the phase-bias difference ϕ_d, as a result of the extra path length Δl, is less (ideally significantly less) than π rad. To meet this condition with a PET film ($n = 1.6$), for example, and 850-nm light emerging from an optical fiber with a maximum half-angle divergence of 5°, the thickness of the film as determined from Eq. (12) should be less than 35 μm.

B. Sensor–Acoustic-Field Interaction: Acoustic Sensitivity and Frequency Response

This subsection concerns the sensor–acoustic-field interactions and considers the phase modulation produced by an acoustic wave incident on the sensing film. The acoustic sensitivity, as a function of frequency, is considered by an examination of the thickness resonance modes arising from reflections of a normally incident acoustic wave within the sensing film only. The effects of radial resonance modes and acoustic perturbations produced by the structure holding the sensing film are not considered.

The strain that is due to a normally incident acoustic wave produces a change in the thickness of the polymer film dl, which then gives rise to a phase shift $d\phi$ which, neglecting strain-induced changes in the refractive index, is

$$d\phi = \frac{4\pi n\, dl}{\lambda}, \tag{13}$$

where n is the refractive index of the polymer film and λ is the wavelength of the laser source. The changes in film thickness is given by

$$dl = \int_0^l \frac{P_T(x, t)}{E}\, dx, \tag{14}$$

where E is the Young's modulus of the polymer film. $P_T(x, t)$ represents the spatial distribution of pressure across the thickness of the sensing film and is the sum of the component of the incident acoustic wave that is transmitted into the sensor film P_1 and subsequent acoustic reflections $P_2, P_3, \ldots, P_n$ at the boundaries of the film. These reflections, shown schematically in Fig. 3, arise as a result of the differences in acoustic impedance between the polymer film and the surrounding media.

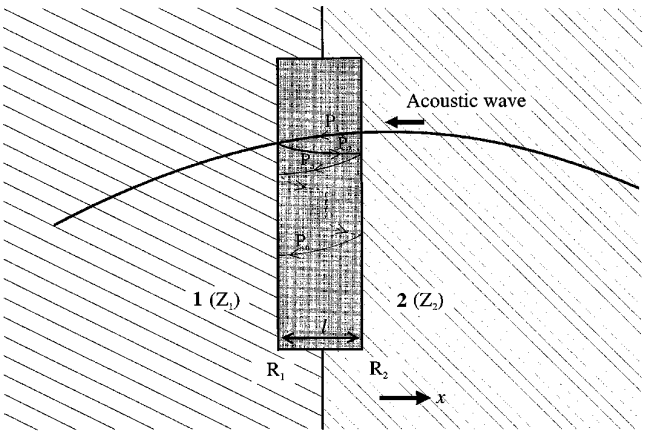

Fig. 3. Acoustic reflections within the sensing film. As in Fig. 2, the numerals denote media 1 and 2.

In general, for a sinusoidally varying incident acoustic wave of amplitude P_0 and angular acoustic frequency ω traveling in the negative x direction, the stress distribution across the film from the superposition of P_1 and an odd number of subsequent reflections N, with the acoustic attenuation neglected, is

$$P_T = P_0 T \sum_{i=0}^{(N-1)/2} \{R_1{}^i R_2{}^i \sin[\omega t - k(2li - x)] + R_1{}^{i+1} R_2{}^i \sin[\omega t - k(2li + x)]\}, \quad (15)$$

where T is the pressure-amplitude transmission coefficient resulting from the acoustic-impedance mismatch between the sensing film and surrounding media, R_1 and R_2 are the pressure-amplitude reflection coefficients at the two surfaces of the film, and

$$T = \frac{2Z}{Z + Z_2}, \quad R_1 = \frac{Z_1 - Z}{Z + Z_1}, \quad R_2 = \frac{Z_2 - Z}{Z + Z_2}, \quad (16)$$

where Z is the acoustic impedance of the polymer sensing film and Z_1 and Z_2 are the acoustic impedances of the media on either side of the film. Substituting P_T into Eq. (14) and evaluating the integral give an expression of the form

$$\mathrm{d}l = \frac{P_0 T}{Ek} \sum_{i=1}^{N+2} \psi_i \cos(\omega t + \xi_i). \quad (17)$$

This is the sum of $N + 2$ sinusoids of the same frequency but different amplitudes and phases and can be written as

$$\mathrm{d}l = \frac{P_0 T}{Ek} \psi \cos(\omega t + \xi), \quad (18)$$

where the amplitude ψ is

$$\psi = \left[\left(\sum_{i=1}^{N+2} \psi_i \cos \xi_i\right)^2 + \left(\sum_{i=1}^{N+2} \psi_i \sin \xi_i\right)^2\right]^{1/2}. \quad (19)$$

The thickness of the sensor film is therefore modulated at a frequency ω and is of an amplitude

$$\mathrm{d}l_0 = \frac{P_0 T}{Ek} \psi. \quad (20)$$

The pressure-amplitude reflection coefficient resulting from the acoustic-impedance mismatch between water (acoustic impedance of 1.5×10^6 kg/m^2 s) and a polymer film such as PET (acoustic impedance of 3.1×10^6 kg/m^2 s) is small at -0.35. For the purposes of modeling the frequency response of the sensor film it is sufficient to consider five reflections because, after this number of reflections, the amplitude is reduced by more than 2 orders of magnitude. After evaluation of Eq. (15) for $N = 5$ and the integral in Eq. (14), Eq. (19) yields

$$\begin{aligned}\psi_{[5]}^2 = {} & [(1 - R_1 + (R_1 - R_2R_1 - 1)\cos kl \\ & + (R_2R_1 - R_2R_1{}^2)\cos 2kl \\ & + (R_2R_1{}^2 - R_2{}^2R_1{}^2)\cos 3kl \\ & + (R_2{}^2R_1{}^2 - R_2{}^2R_1{}^3)\cos 4kl + R_2{}^2R_1{}^3 \cos 5kl]^2 \\ & + [(R_2R_1 - R_1 - 1)\sin kl - (R_2R_1 - R_2R_1{}^2)\sin 2kl \\ & - (R_2R_1{}^2 - R_2{}^2R_1{}^2)\sin 3kl \\ & - (R_2{}^2R_1{}^2 - R_2{}^2R_1{}^3)\sin 4kl - R_2{}^2R_1{}^3 \sin 5kl]^2. \end{aligned} \quad (21)$$

The acoustic sensitivity of the sensing film can be conveniently defined as the phase modulation per unit acoustic pressure $\mathrm{d}\phi_0/P_0$. For $N = 5$ this is

$$\frac{\mathrm{d}\phi_0}{P_0} = \frac{4\pi n}{\lambda} \frac{T}{Ek} \psi_{[5]}. \quad (22)$$

Equation (22) can be used to predict the sensitivity and the frequency response for various sensor-film materials and different media in contact with the two sides of the film. Four different acoustic-loading configurations are considered below. The acoustic sensitivity as a function of acoustic frequency for each case is shown in Fig. 4 for a 50-μm-thick PET film that has the values $E = 4.4$ GPa, $c = 2200$ m/s, and $n = 1.6$.

1. *Matched-Load Sensing Film*

A matched load represents an ideal case in which the polymer film is surrounded by media of the same acoustic impedance ($Z = Z_1 = Z_2$) so there are no acoustic reflections at the boundaries. Under these conditions $R_1 = R_2 = 0$ and $T = 1$, and Eq. (21) reduces to

$$\psi_{[5]} = 2 \sin\left(\frac{kl}{2}\right). \quad (23)$$

Inserting Eq. (23) into Eq. (22) and using the relation $k = 2\pi/\lambda_a$, where λ_a is the acoustic wavelength, we find that the acoustic sensitivity is

$$\frac{\mathrm{d}\phi_0}{P_0} = \frac{4n}{\lambda} \frac{\lambda_a}{E} \sin\left(\frac{\pi l}{\lambda_a}\right). \quad (24)$$

There are two frequency regimes of interest. First, there is the case in which the acoustic wavelength λ_a is much greater than the thickness l of the film, and second there is the case when λ_a approaches l. If λ_a is large compared with l, the pressure gradient across the sensor is effectively zero and Eq. (24) reduces to, for $\lambda_a \gg l$,

$$\frac{\mathrm{d}\phi_0}{P_0} = \frac{4\pi n}{\lambda} \frac{l}{E}. \quad (25)$$

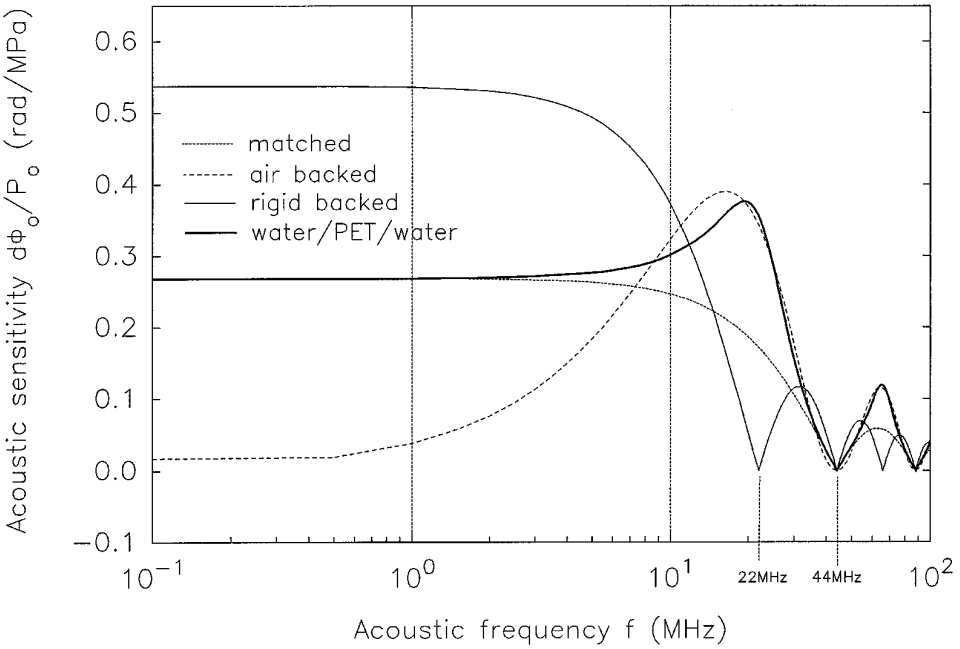

Fig. 4. Theoretical acoustic sensitivity as a function of the frequency response for different acoustic-loading configurations with a 50-μm-thick PET sensing film. Parameters: $E = 4.4$ GPa, $c = 2200$ m/s, $\lambda = 850$ nm, and $Z = 3.1 \times 10^6$ kg/m^2 s.

Equation (25) shows that, at low frequencies and for a given laser wavelength and refractive index n, $d\phi_0/P_0$ is dependent on only the thickness and the Young's modulus of the sensor material. As the acoustic wavelength is reduced and approaches l, the spatial variation of the pressure field across the sensor becomes significant and $d\phi_0/P_0$ decreases, becoming zero when $\lambda_a = l$. The first frequency at which $d\phi_0/P_0$ is zero is given by

$$f_c = c/l, \tag{26}$$

where c is the speed of sound in the sensor material. Beyond f_c the value of $d\phi_0/P_0$ varies rapidly with an increasing frequency and becomes zero for wavelengths equal to multiples of l. In the example shown in Fig. 4 this behavior is shown with f_c occurring at 44 MHz. This simple analysis provides an insight into the required acoustic properties of the sensing element. For the maximum acoustic sensitivity and frequency response, a material with both a low Young's modulus and a high speed of sound is required. A material with a very low Young's modulus will exhibit a high acoustic sensitivity for $\lambda_a \gg l$. If it also has a very low speed of sound then Eq. (12) shows that, for a high-frequency response, l must be small. This small value of l in turn reduces the acoustic sensitivity.

2. Rigid-Back Sensing Film

The sensing film is backed with a medium that has a very high acoustic impedance ($Z_1 \gg Z$) and $R_1 = 1$. For algebraic simplicity the front-face reflection is neglected by setting the values $R_2 = 0$ and $T = 1$ and, from Eq. (21), $\psi_{[5]}$ becomes

$$\psi_{[5]} = 2 \sin kl, \tag{27}$$

and the acoustic sensitivity is

$$\frac{d\phi_0}{P_0} = \frac{4n}{\lambda} \frac{\lambda_a}{E} \sin\left(\frac{2\pi l}{\lambda_a}\right). \tag{28}$$

In the low-frequency limit Eq. (28) reduces, for $\lambda_a \gg l$, to

$$\frac{d\phi_0}{P_0} = \frac{8\pi n}{\lambda} \frac{l}{E}. \tag{29}$$

This expression is a factor of 2 higher than the acoustic sensitivity of the matched-load configuration discussed in Subsection 3.B.1., although the cutoff frequency f_c has decreased by a factor of 2 and now occurs at

$$f_c = c/2l. \tag{30}$$

This change is shown in Fig. 4 occurring at 22 MHz.

3. Air-Backed Sensing Film

In this case the film is backed by air ($Z_1 \ll Z$) so that $R_1 = -1$. To simplify Eq. (21) we again neglect the reflection from the front face of the sensing film by setting $R_2 = 0$ and $T = 1$. Equation (21) becomes

$$\psi_{[5]} = 4 \sin^2 kl, \tag{31}$$

and from Eq. (22) the acoustic sensitivity is

$$\frac{d\phi_0}{P_0} = \frac{8n}{\lambda} \frac{\lambda_a}{E} \sin^2\left(\frac{\pi l}{\lambda_a}\right). \tag{32}$$

The nonuniform frequency-response characteristic of this configuration is shown clearly in Fig. 4, with

the acoustic sensitivity rising from zero to a maximum. Such a configuration gives a poor representation of the acoustic wave, particularly when sensing short pulses with a broadband frequency content.[19]

4. Water–PET–Water Sensing Film

The closest practical configuration to the matched-load ideal described in Subsection 3.B.1. is to have water in contact with both sides of the PET sensing film. In this case $Z_1 = Z_2 = 1.5 \times 10^6$ kg/m^2 s, so that $R_1 = R_2 = -0.35$. The acoustic sensitivity is modeled by the use of the full form of Eq. (21). The prominent features of the frequency-response curve shown in Fig. 4 are the $\lambda/2$ resonance at approximately 20 MHz and the cutoff frequency f_c at 44 MHz. In practice it can be expected that the effects of attenuation within the film (not considered in this model) would act to reduce the magnitude of the $\lambda/2$ resonance. In the low-frequency regime where $\lambda_a \gg l$ and when $R_1 = R_2$, Eq. (21) reduces to

$$\psi_{[5]} = kl \sum_{i=0}^{5} {R_1}^i = \frac{kl(1 - {R_1}^6)}{1 - R_1}, \tag{33}$$

which for small values of R_1 further reduces to

$$\psi_{[5]} = \frac{kl}{1 - R_1} = \frac{kl}{T}. \tag{34}$$

Substituting Eq. (34) into Eq. (22) gives

$$\frac{\mathrm{d}\phi_0}{P_0} = \frac{4\pi n}{\lambda}\frac{l}{E}, \tag{35}$$

which is the same expression for the low-frequency acoustic sensitivity for the matched-load case given in Eq. (25). This behavior is shown clearly in Fig. 4, with the departure from the matched-load case beginning at approximately 2 MHz. The low-frequency acoustic sensitivity of the water–PET–water configuration is 0.27 rad/MPa.

C. Overall System Sensitivity

The essential point to be noted from Subsection 3.A. is that the phase sensitivity is limited by the maximum laser power that can be used before the dc level saturates the photodiode. To achieve the highest phase sensitivity we have established that (1) the dc level should be kept to a minimum by ensuring that the fringe visibility is equal to one, and (2) the interferometer thickness and the angle of divergence of the optical fiber should be kept to a minimum. Thus the thickness of the sensing element is not determined solely by considerations of the acoustic sensitivity and the frequency response, as might be expected. For example, if a low-frequency response is required, the film could be made quite thick to achieve a high acoustic sensitivity. This, however, would increase the signal-canceling problems arising from optical-fiber illumination of the sensing film and would degrade the overall sensitivity. The trade-off is therefore between the requirements of phase sensitivity, acoustic sensitivity, and frequency response. When the very highest sensitivity is required for detecting small-amplitude signals, it is necessary to strive for both the highest possible acoustic and phase sensitivities. Under high-amplitude-signal conditions it is important to ensure that the acoustic sensitivity is not too high. If the signal-induced phase modulation becomes too large, the small-angle approximation cannot be invoked, resulting in a nonlinear response. In such circumstances it is the phase sensitivity that should be optimized for the maximum dynamic range.

Multiplying the phase sensitivity and the acoustic sensitivity brings together the interferometric and acoustic aspects of the sensor operation to give an expression for the overall system sensitivity in terms of the intensity per unit acoustic pressure. Multiplying Eq. (22) by Eq. (9) yields

$$\frac{\mathrm{d}I_0}{P_0} = \frac{8\pi n I(1 - r_1)\sqrt{r_1 r_2}\,T\psi_{[5]}}{Ek\lambda}. \tag{36}$$

For a 50-μm PET sensing film surrounded by water with the use of the values 50.4 μW/rad for the phase sensitivity obtained in Subsection 3.A. and 0.27 rad/MPa for the acoustic sensitivity obtained in Subsection 3.B., Eq. (36) gives the system sensitivity at 13.6 μW/MPa.

4. Experimental Procedure

The aim of the experimental work was to demonstrate the concept of the optical-fiber Fabry–Perot polymer-film ultrasound sensor. An experimental sensor head has been constructed and tested to evaluate the performance of a 50-μm PET film acting as the sensing element. Laser-generated thermoelastic waves were used as a source of wideband ultrasound, and the output of the sensor was compared with that of a PVDF-membrane hydrophone.

A. Experimental Sensor Head

The sensor head was designed so that the sensing film could be easily removed and replaced, the fiber–film separation varied, and different areas of the film interrogated for phase-bias control. The latter is necessary because, for the purpose of demonstrating the concept, a fixed-wavelength He–Ne laser was used rather than a tunable laser diode source. The sensor head, shown in Fig. 5, was

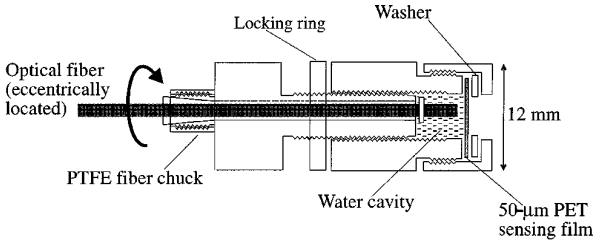

Fig. 5. Illustration of the experimental sensor head.

constructed from brass and is of an overall diameter of 12 mm. The sensing film used was 50-μm-thick PET film. This thickness was chosen as an acceptable compromise between the requirements of acoustic sensitivity and of limiting the signal-canceling effects described in Section 3. The optical fiber is inserted through an eccentrically located hole in a polytetrafluoroethylene (PTFE) insert in the main screw, which permits it to be rotated without gripping the fiber. A plastic disk is bonded to the fiber a few millimeters from its distal end. Turning the screw advances the fiber toward the film, and a locking ring enables the screw to be locked at the appropriate fiber–film separation. The fiber is eccentrically located, so rotation of the screw results in the light emerging from the end of the fiber scanning a circle on the polymer film. Because a typical polymer film is not perfectly flat, the phase bias is different for each point on the film that is illuminated. Exploiting this fact provides a means of setting the interferometer at quadrature. First the main screw was rotated until it had passed through two consecutive points that produced a signal minimum. The screw was then turned back until the illuminated region of the film was at a point equidistant between the two points corresponding to the signal minima. At this point the interferometer was at quadrature, and the signal at a maximum. The experimental sensor head described above was designed primarily for evaluation purposes and is somewhat large for certain applications. A 1-mm-diameter sensor head with the same sensing element has been incorporated into a photoacoustic probe,[20] demonstrating the feasibility of a miniature-probe-type configuration.

B. Experimental Arrangement and Method

The experimental arrangement is shown in Fig. 6. Wideband ultrasonic thermoelastic waves were generated by the absorption of 20-ns optical pulses at 532 nm in Quink Solv-x ink, which was assumed to approximate a nonscattering absorber. The optical-beam diameter was 4 mm. The optical pulses, produced by a frequency-doubled Q-switched Nd:YAG laser, were directed onto the ink, which was placed in contact with the Perspex window in the bottom of the water bath. The resulting thermoelastic waves propagate vertically upward and are reflected from a glass block angled at 45° acting as an acoustic reflector. A calibrated 25-MHz, 50-μm bilaminar PVDF-membrane hydrophone with an active diameter of 1 mm and which was immersed in the water bath was used as a reference hydrophone. This type of hydrophone is widely acknowledged as the gold standard in ultrasound measurements on account of its wideband, uniform frequency response, linearity and stability, and minimum perturbation to the acoustic field under measurement. The calibration of the hydrophone, carried out by the National Physical Laboratory, is over the range of 1–30 MHz in steps of 1 MHz. A 7-mW He–Ne laser operating at 633 nm was used to illuminate the sensor film by means of a 2-m length of 400-μm all-silica optical fiber. The intensity-modulated signal reflected from the sensor film was transmitted back along the fiber and directed onto a 25-MHz silicon p.i.n. hybrid photodiode with an active diameter of 0.8 mm.

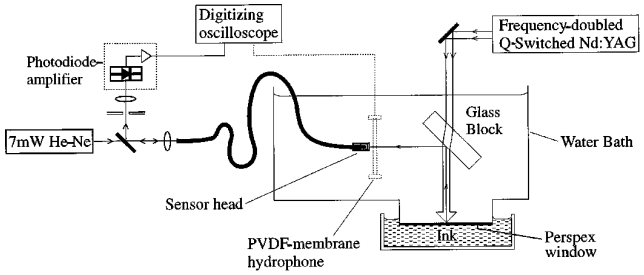

Fig. 6. Experimental arrangement for measuring the sensor performance.

Experiments were carried out to measure the sensitivity, frequency response, linearity, and stability of the optical-fiber sensor. For the experiments in which linearity and stability were being measured, the sensor head was positioned directly behind the hydrophone in the water tank so that the same region in the acoustic field was measured simultaneously by both devices. For the sensitivity and frequency-response measurements, even the relatively small acoustic perturbation produced by the membrane hydrophone was unacceptable. We therefore obtained these measurements by immersing the optical-fiber sensor in the tank, taking a measurement, and then removing the sensor and replacing it with the hydrophone. To ensure that the same point in the ultrasound field was being measured by both the sensor and the hydrophone, the low-power, fixed-Q output of the Nd:YAG laser was used as an alignment beam. The position of the hydrophone or sensor was adjusted until the Fresnel reflection from the Perspex window was visible in the active area of the device. Fine adjustment was then carried out by steering the optical beam while thermoelastic waves were being generated in the liquid absorber until the output of the device under alignment was at a maximum. In addition, care was taken to ensure that the acoustic path length (approximately 6 cm) traveled by the thermoelastic wave was identical for both measurements. This was achieved to a high degree of accuracy by the adjustment of the position of each device so that the time from firing the Q-switched laser pulse to detection of the thermoelastic wave was the same. There is significant variation from pulse to pulse in the output of a Q-switched Nd:YAG laser, so the output from each device was averaged over 60 shots by means of the signal-averaging function of a 500-MHz digitizing oscilloscope.

C. Sensor Mode of Operation

In principle it is possible that the signal detected by the sensor is due to acoustically induced bulk move-

ment or displacement of the sensing film. In this case it would be the Fresnel reflections from the cleaved distal end of the fiber and the front face of the film (the side closest to the end of the fiber) that would interfere. Verification that it was changes in the thickness of the sensing film that were being detected rather than its bulk displacement was achieved when the sensor was set up and aligned so that a clearly detectable acoustic signal could be observed. The back face of the film (the side furthest from the fiber) was then abraded with sandpaper, thus destroying the specular reflection from the back face. The only significant interference would then be between the reflections from the end of the optical fiber and the front face of the polymer film. Under these conditions no signal from an incident acoustic wave could be detected, verifying the thickness mode of operation of the sensor.

D. PVDF-Membrane Hydrophone and Sensor Comparison

The signals measured by the optical-fiber sensor and the hydrophone are shown in Figs. 7. A measurement was made first with the optical sensor. The sensor was then removed and replaced with the membrane hydrophone as described in Subsection 4.B. so that the same point in the acoustic field was measured with both devices. Signal averaging over 60 pulses was performed in each case. The first signal, A (see Figs. 7), is a small-amplitude thermoelastic wave generated at the boundary between the upper surface of the Perspex window and the surrounding water. The second signal B is the thermoelastic wave generated in the ink. Signal C is the reflection of signal A within the Perspex window. Signal R [Fig. 7(a)] is the reflection of the thermoelastic-wave signal B from the tip of the optical fiber (showing that the fiber–film separation is approximately 1.6 mm) and therefore appears on only the sensor output. These results indicate that the sensor exhibits a signal-to-noise ratio comparable with that of the membrane hydrophone. In addition, the shape of the wave measured by the sensor, as shown more clearly in the normalized, expanded view of signal B in Fig. 8, is in good agreement with that of the hydrophone, suggesting comparable frequency-response characteristics.

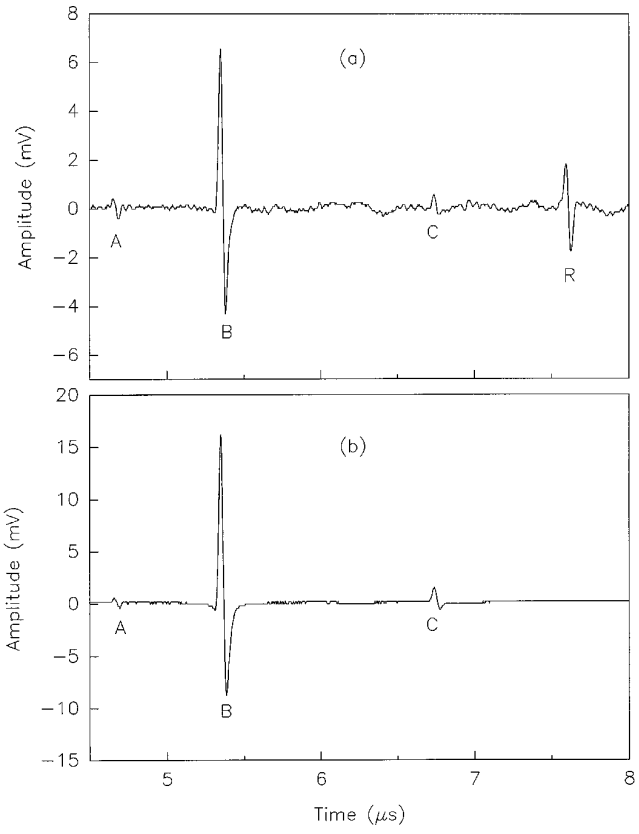

Fig. 7. Comparison of (a) the optical-fiber sensor output with (b) the 50-μm PVDF-membrane hydrophone output in response to a thermoelastic wave of amplitude 0.1 MPa. Signal labels: A, thermoelastic wave generated in the Perspex window; B, thermoelastic wave generated in the ink absorber; C, reflection of signal A within the Perspex window; R, reflection of signal B from the tip of the optical fiber.

1. *Sensitivity*

The end-of-cable sensitivity of the membrane hydrophone is 150 mV/MPa at 10 MHz. By direct comparison of the peak positive pressures registered by each device as shown in Figs. 7, the sensitivity of the sensor is 61 mV/MPa. The sensitivity of the photodiode–amplifier combination is 10 mV/μW, so this value corresponds to a system sensitivity dI_0/P of 6.1 μW/MPa. If we take into account that the laser power is 7 mW and the wavelength is 633 nm, dI_0/P is approximately a factor of 5 lower than the value predicted in Section 3 for normally incident light. The reason for this lower value is most likely due to the signal-canceling effects resulting from the divergent output of the optical fiber, which reduces and limits the phase sensitivity. The Fresnel reflections that fall on the photodiode from the front and the distal cleaved ends of the fiber further exacerbate this problem by adding to the dc level.

2. *Noise*

The noise floor of the membrane hydrophone is very low[21] (less than 0.5 KPa) and in these measurements is dominated by the noise associated with the oscilloscope. It is measured, in this example, over 60 averages at 0.050 mV (0.33 KPa) in a measurement bandwidth of 25 MHz. The corresponding measurement for the sensor, dominated by the photodiode–amplifier-combination noise, over the same measurement bandwidth is 0.14 mV (2.30 KPa). Thus in terms of the signal–noise ratio the sensor output is approximately a factor of 7 lower than the PVDF-membrane hydrophone.

3. *Frequency Response*

We obtained the frequency response by taking the Fourier transform $B_s(f)$ of the normalized signal in Fig. 8 that was measured with the sensor. The Fourier transform of the corresponding signal as

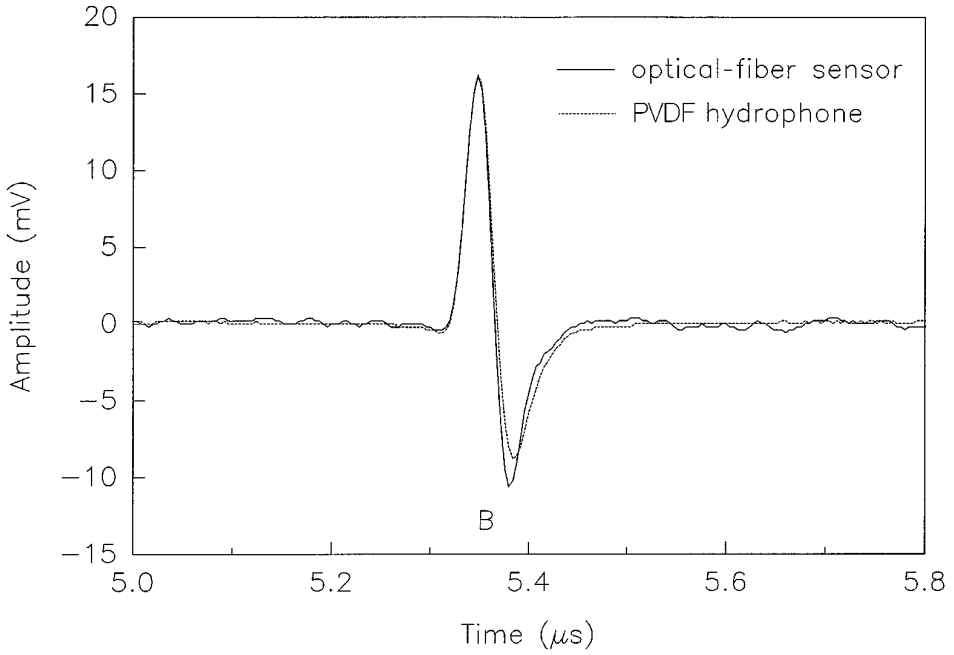

Fig. 8. Expanded view of signal B from Figs. 7 showing the comparison of the normalized optical-fiber sensor output with the PVDF-membrane hydrophone output.

measured with the hydrophone $B_h(f)$ was then computed, and a correction was applied to take into account the frequency-response characteristics of the hydrophone, giving $C_h(f)$, as shown in Fig. 9. $C_h(f)$ gives the distribution of frequency components arriving at the sensor head. Dividing $B_s(f)$ by $C_h(f)$ therefore gives the frequency response of the sensor, as shown in Fig. 10. The theoretical frequency response (given in Section 3) for the 50-μm PET film surrounded by water is also shown, along with the calibrated frequency response of the PVDF-membrane hydrophone. At low frequencies the correlation between theory and experiment is good. The half-wave resonance appears as expected at approximately 20 MHz, although its magnitude is a factor of 1.4 larger than expected. Although it was not terminated at 50 Ω, the length of the coaxial cable (0.6 m) connecting the hybrid photodiode to the oscilloscope should not have produced a resonance close to this frequency. Further investigation showed that it was a peak in the frequency response of the photodiode–amplifier combination that coincided with the 20-MHz acoustic-thickness-mode resonance that was responsible for the apparent enhanced resonance, and, in the time domain, for the increased size of the rarefaction part of the signal as compared with the hydrophone output that is shown in Fig. 8. Careful choice of a detector with a uniform response and a matched electrical load would overcome this problem.

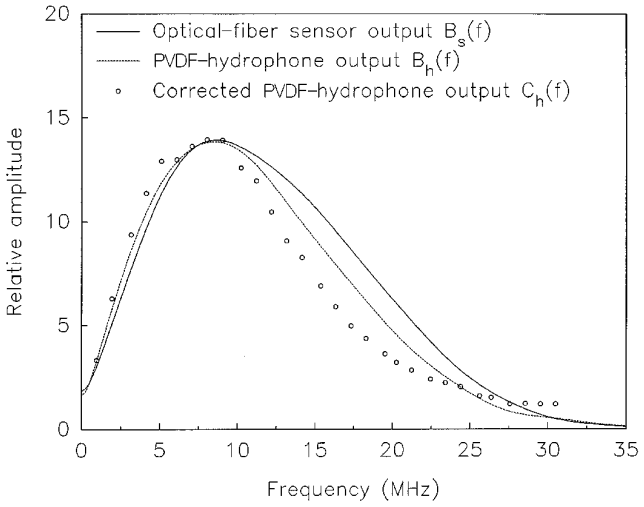

Fig. 9. Acoustic frequency spectra of the signals measured with the optical-fiber sensor and the PVDF-membrane hydrophone shown in Fig. 8.

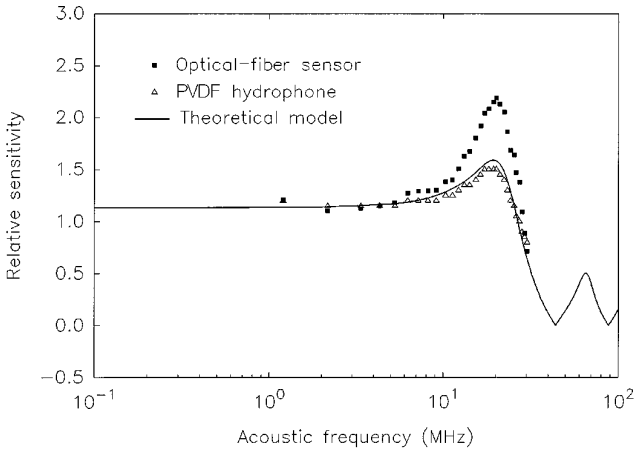

Fig. 10. Comparison of the optical-fiber-sensor frequency response with the theoretical model and the PVDF-membrane-hydrophone frequency-response values.

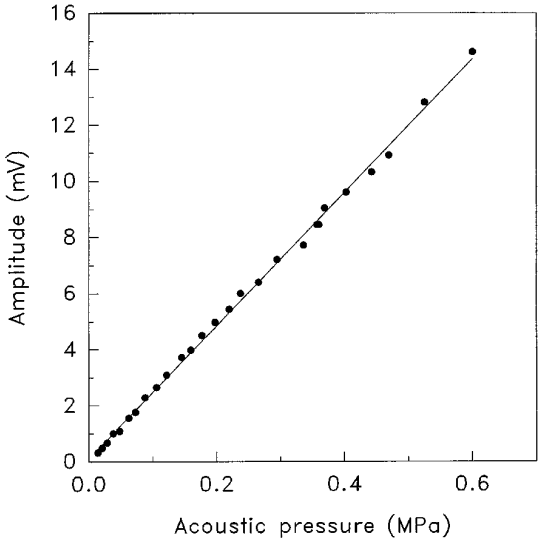

Fig. 11. Optical-fiber sensor output as a function of the acoustic pressure as measured with the PVDF-membrane hydrophone.

4. *Linearity*

It is assumed that the PVDF-membrane hydrophone is linear to well beyond 0.6 MPa.[21,22] The sensor was placed directly behind the hydrophone, and the positions of both devices adjusted independantly until the maximum signal detected by each was observed. Simultaneous readings from the sensor and the hydrophone were taken. This procedure was repeated over a range of acoustic pressures by variation of the energy of the optical pulses incident upon the ink absorber. The results, shown in Fig. 11, show an excellent linearity of response up to 0.5 MPa, limited by the maximum pulse energy of the *Q*-switched Nd:YAG laser. A dynamic range in excess of 30 dB was obtained. It should be noted that the acoustic pressures shown in Fig. 11 are those measured with the hydrophone. The true acoustic pressure arriving at the sensor head is somewhat lower as a result of the attenuation of the acoustic signal as it passes through the hydrophone.

5. *Stability*

Adequate short- and long-term stabilities are essential for a practical measurement device. The usual source of sensitivity fluctuations in homodyne interferometric sensors is due to environmentally induced variations in the phase bias, particularly in the case of long-path interferometers. In the scheme presented here the thinness of the polymer film acting as the interferometer means that it is relatively insensitive to external perturbations that are likely to occur in the short term. The sensitivity over a period of 80 h is shown in Fig. 12. The experimental method was the same as that used for the linearity measurements. Figure 12 shows that the sensor is stable, within the uncertainty of the measurement, typically over a period of several hours, and over 80 hours the output does not fluctuate by more than 10%. This stability indicates a low sensitivity to ambient temperature and pressure fluctuations.

Other significant factors that may lead to changes in sensitivity are those influences that act on the optical-fiber downlead. Vibration produced when the fiber was rapidly and vigorously shaken had virtually no effect on the signal. The signal was, however, observed to decrease when the fiber was bent to a significant degree. Effectively the higher-order modes (which remain unfilled over a short length of the fiber) become filled when the fiber is bent, increasing the angle of divergence of the light emerging from the end of the fiber and thus bringing into effect the signal-canceling effects described in Subsection 3.A.2. This effect was reduced when the modes were scrambled and the input launch conditions adjusted so that all the propagation modes were filled, resulting in a constant angle of divergence. This improvement however is obtained at the expense of phase sensitivity.

E. Rigid-Backed Sensing Film

It would be useful to find some way to remove the reflection of the thermoelastic wave (signal R in Figs.

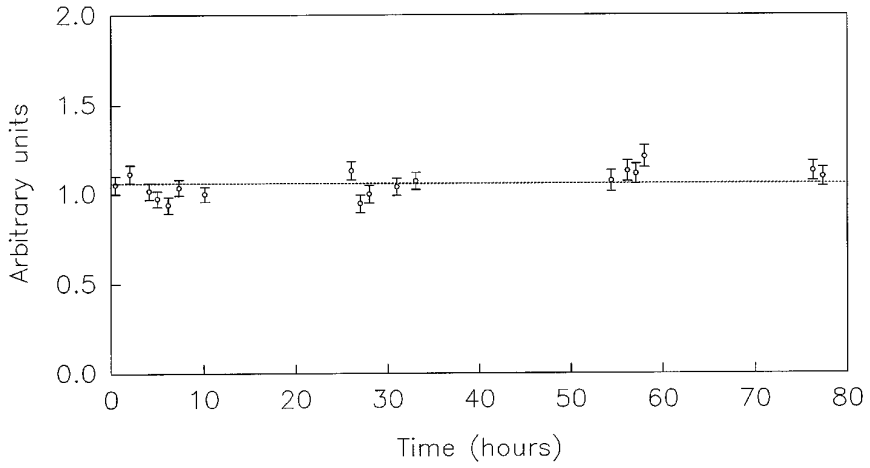

Fig. 12. Variation of optical-fiber sensor output with time.

7) from the tip of the fiber. This reflection may coincide with the arrival of a signal to be detected and can affect the low (<1 MHz) frequency response of the sensor. A rigid backing offers a solution as it gives a high acoustic sensitivity and a uniform, although reduced, frequency response. It could conceivably be achieved by the attachment of a transparent material of relatively high acoustic impedance, such as glass, to the back of the sensing film. This solution, however, would destroy the fringe visibility because the Fresnel reflection coefficient between PET and glass is very low (1×10^{-3}). A novel approach has been found to overcome the reduction in fringe visibility if it is ensured that there is a gap between the film and the backing that, in acoustic terms, is of negligible thickness but is large enough to allow a thin layer of water to exist. The water layer maintains the fringe visibility at unity but allows the sensor to be effectively rigid backed. In practice this rigid backing was achieved by the use of the cleaved end of the fused-silica optical fiber as the backing material. The fiber was moved gradually closer toward the sensing film until the thermoelastic waves reflected from the tip of the fiber were superposed onto the initial wave incident on the sensor film. The effect of this superposition is to increase the acoustic sensitivity by a factor of 2, as shown in the theoretical model shown in Fig. 4. This result is verified in Figs. 13, which show the output of the sensor before and after the fiber is brought close to the sensing film. Some broadening of the second half of the pulse is apparent in Fig. 13(b) because of the reduced frequency response of the rigid-backed configuration.

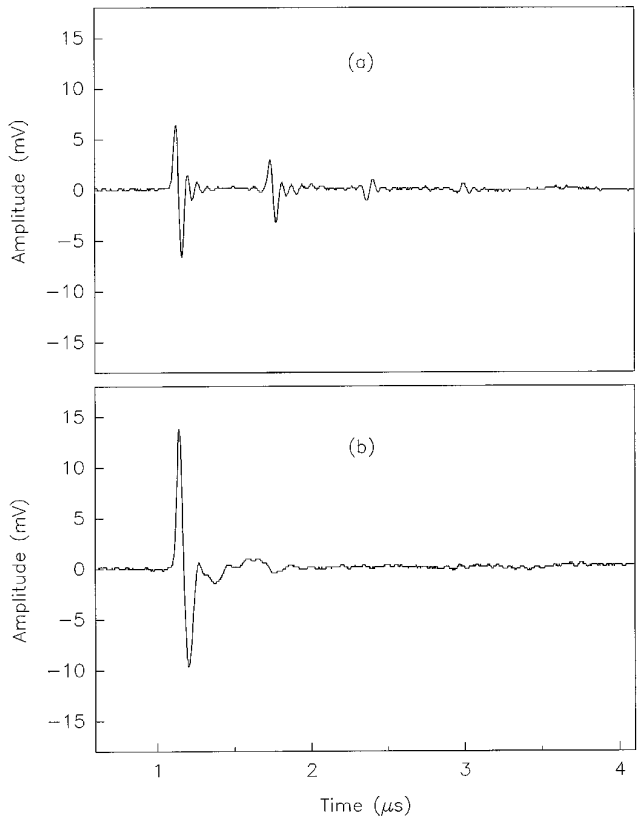

Fig. 13. (a) Water-backed configuration showing multiple reflections between the sensing film and the fiber tip, and (b) superposition of the same reflections in a rigid-backed configuration.

5. Conclusions

An extrinsic optical-fiber sensor has been described and demonstrated, showing that a thin polymer film acting as a Fabry–Perot interferometer can be used for the detection of ultrasound. High sensitivity and a flat, wideband frequency response have been demonstrated to be in good agreement with a theoretical model. The sensor was found to exhibit a performance comparable with that of a PVDF-membrane hydrophone.

It is considered that for practical use two aspects require further attention. First, a tunable laser diode would be needed to set the phase bias to quadrature on start up and to maintain the bias for high stability. Second, reducing the sensitivity to bends in the fiber without lowering the phase sensitivity is required. Reduced bend sensitivity has been demonstrated by the use of mode scrambling, but it reduces the ratio of the phase sensitivity to the dc level. This ratio could be increased if the distal end of the fiber were mode stripped to reduce the angle of divergence. Such a measure would significantly reduce the light emerging from the end of the fiber. A higher laser power would be needed to compensate the reduction in emergent light, or alternatively more efficient use of the light could be made by the application of optically reflective coatings to the two sides of the sensing film.

A particular advantage with this technology is that there are a wide range of optically clear polymer films of varying acoustic properties that could be used as the sensing film. This availability enables the properties of the sensing film to be chosen in accordance with the requirements of a specific application. For example, if a very flat frequency response is required, a polymer that has an acoustic impedance even closer to water than that of PET could be chosen to minimize the thickness resonance. If a high acoustic sensitivity is required, a material with a low Young's modulus can be selected. In addition, because polymer films of the order of a few micrometers thick are readily available, potential bandwidths of several hundred megahertz are possible. Furthermore, because the active area of the sensor is defined by the spot size illuminating the sensing film, very small active diameters (a few tens of micrometers) can be obtained by the use of small-diameter fibers. For example, a 50-μm-diameter fiber could easily be employed, giving an excellent spatial resolution and a low directional sensitivity. This potential for high performance makes it particularly suitable for the measurement of the output of medical ultrasound equipment. For such measurements, an inexpensive sensor is required that gives an accurate temporal and spatial representation of

the ultrasound field under measurement. Application may also be found in situations in which high levels of electromagnetic interference preclude the use of conventional piezoelectric devices and limited access requires an inexpensive, miniature, flexible probe.

This work has been supported by the British Heart Foundation and the Medical Research Council.

References and Note

1. R. P. De Paula, L. Flax, J. H. Cole, and J. A. Bucaro, "Single mode fiber ultrasonic sensor," IEEE J. Quantum Electron. **QE-18,** 680–683 (1982).
2. H. L. W. Chan, K. S. Chiang, D. C. Price, J. L. Gardner, and J. Brinch, "Use of a fiber-optic hydrophone in measuring acoustic parameters of high power hyperthermia transducers," Phys. Med. Biol. **34,** 1609–1622 (1989).
3. H. L. W. Chan, K. S. Chiang, D. C. Price, and J. L. Gardner, "The characterisation of high frequency ultrasonic fields using a polarimetric optical fiber sensor," J. Appl. Phys. **66,** 1565–1570 (1989).
4. K. S. Chiang, H. L. W. Chan, and J. L. Gardner, "Detection of high frequency ultrasound with a polarisation maintaining fiber," J. Lightwave Technol. **8,** 1221–1227 (1990).
5. L. Liu and R. M. Measures, "Detection of high-frequency elastic waves with embedded ordinary single mode fibers," in *Fiber Optics and Laser Sensors IX,* R. P. De Paula and E. Udd, eds., Proc. Soc. Photo-Opt. Instrum. Eng. **1584,** 226–232 (1991).
6. N. Narendram, C. Zhou, S. Letcher, and A. Shukla, "Fiber-optic acoustic sensor for nondestructive evaluation," Opt. Lasers Eng. **22,** 137–148 (1995).
7. R. P. De Paula, J. H. Cole, and J. A. Bucaro, "Broad-band ultrasonic sensor based on induced optical phase shifts in single mode fibers," J. Lightwave Technol. **LT-1,** 390–393 (1983).
8. N. Lagakos, A. Dandridge, J. H. Cole, A. B. Tveten, and J. A. Bucaro, "Ultrasonic acoustic sensing," in *Automotive Displays and Industrial Illumination,* B. Chang and T. M. Lemons, eds., Proc. Soc. Photo-Opt. Instrum. Eng. **798,** 94–101 (1987).
9. J. J. Alcoz, C. E. Lee, and H. F. Taylor, "Embedded fiber-optic Fabry–Perot ultrasound sensor," IEEE Trans. Ultrason. Ferroelectr. Freq. Control **37,** 302–305 (1990).
10. S. Knudsen and K. Blotekjae, "An ultrasonic fiber-optic hydrophone incorporating a push–pull Sagnac interferometer," J. Lightwave Technol. **12,** 1696–1700 (1994).
11. D. A. Jackson, R. Priest, A. Dandridge, and A. B. Tveten, "Elimination of drift in a single-mode optical fiber interferometer using a piezoelectrically stretched coiled fiber," Appl. Opt. **19,** 2926–2929 (1980).
12. See, for example, D. W. Stowe, D. R. Moore, and R. G. Priest, "Polarization fading in fiber interferometric sensors," IEEE J. Quantum Electron. **QE-18,** p. 1644 (1982).
13. T. A. Tran, W. V. Miller, K. A. Murphy, M. Vengsarkar, and R. O. Claus, "Stabilized extinsic fiber-optic Fizeau sensor for surface acoustic wave detection," J. Lightwave Technol. **10,** 1499–1505 (1992).
14. D. P. Hand, S. Freeborn, P. Hodgson, T. A. Carolan, K. M. Quan, H. A. Mackenzie, and J. D. C. Jones, "Optical-fiber interferometry for photoacoustic spectroscopy in liquids," Opt. Lett. **20,** 213–215 (1995).
15. D. R. Bacon, "Primary calibration of ultrasonic hydrophones using optical interferometry," IEEE Trans. Ultrason. Ferroelectr. Freq. Control **35,** 152–161 (1988).
16. B. A. Williams and R. J. Dewhurst, "Differential fiber-optic sensing of laser generated ultrasound," Electron. Lett. **31,** 391–392 (1995).
17. Y. Wu, P. M. Shankar, P. A. Lewin, and D. P. Koller, "Fiber optic ultrasonic sensor using Raman–Nath light diffraction," IEEE Trans. Ultrason. Ferroelectr. Freq. Control **41,** 166–171 (1994).
18. B. Granz, R. Holzapfel, and G. Kohler, "Measurement of shockwaves in the focus of a lithotripter," Proc. IEEE 991–994 (1989).
19. P. C. Beard and T. N. Mills, "An optical fiber sensor for the detection of laser generated ultrasound in arterial tissues," in *Medical Sensors II and Fiber Optic Sensors,* A. V. Scheggi, F. Baldini, P. R. Coulet, and O. S. Wolfbeis, eds., Proc. Soc. Photo-Opt. Instrum. Eng. **2331,** 112–122 (1994).
20. P. C. Beard and T. N. Mills, "Evaluation of an optical fiber probe for in vivo measurement of the photoacoustic response of tissues," in *Advances in Fluorescence Sensing Technology II,* J. R. Lakowicz, eds., Proc. Soc. Photo-Opt. Instrum. Eng. **2388,** 446–457 (1995).
21. R. C. Preston, D. R. Bacon, A. J. Livett, and K. Rajendran, "PVDF membrane hydrophone performance properties and their relevance to the measurement of the acoustic output of medical ultrasound equipment," J. Phys. E **16,** 786–796 (1983).
22. P. A. Lewin, "Practical implementations and technology of measurement devices," in *Ultrasonic Exposimetry,* M. C. Ziskin and P. A. Lewin, eds. (CRC Press, Boca Raton, Fla., 1993), Chap. 7, pp. 195.